THE JOURNAL OF BIOLOGICAL CHEMISTRY
Vol. 276, No. 4, Issue of January 26, pp. 2354–2360, 2001
Printed in U.S.A.

2′-*O*,4′-*C*-Methylene Bridged Nucleic Acid Modification Promotes Pyrimidine Motif Triplex DNA Formation at Physiological pH

THERMODYNAMIC AND KINETIC STUDIES*

Received for publication, August 25, 2000, and in revised form, October 5, 2000
Published, JBC Papers in Press, October 16, 2000, DOI 10.1074/jbc.M007783200

Hidetaka Torigoe‡§, Yoshiyuki Hari¶, Mitsuaki Sekiguchi¶, Satoshi Obika¶, and Takeshi Imanishi¶‖

From the ‡Tsukuba Life Science Center, Institute of Physical and Chemical Research (RIKEN), Ibaraki 305-0074, Japan and ¶Graduate School of Pharmaceutical Sciences, Osaka University, Osaka 565-0871, Japan

Extreme instability of pyrimidine motif triplex DNA at physiological pH severely limits its use in an artificial control of gene expression *in vivo*. Stabilization of the pyrimidine motif triplex at physiological pH is, therefore, crucial in improving its therapeutic potential. To this end, we have investigated the thermodynamic and kinetic effects of our previously reported chemical modification, 2′-*O*,4′-*C*-methylene bridged nucleic acid (2′,4′-BNA) modification of triplex-forming oligonucleotide (TFO), on pyrimidine motif triplex formation at physiological pH. The thermodynamic analyses indicated that the 2′,4′-BNA modification of TFO increased the binding constant of the pyrimidine motif triplex formation at neutral pH by ~20 times. The number and position of the 2′,4′-BNA modification introduced into the TFO did not significantly affect the magnitude of the increase in the binding constant. The consideration of the observed thermodynamic parameters suggested that the increased rigidity itself of the 2′,4′-BNA-modified TFO in the free state relative to the unmodified TFO may enable the significant increase in the binding constant at neutral pH. Kinetic data demonstrated that the observed increase in the binding constant at neutral pH by the 2′,4′-BNA modification of TFO resulted from the considerable decrease in the dissociation rate constant. Our results certainly support the idea that the 2′,4′-BNA modification of TFO could be a key chemical modification and may eventually lead to progress in therapeutic applications of the antigene strategy *in vivo*.

In recent years, triplex DNA has attracted considerable interest because of its possible biological functions *in vivo* and its wide variety of potential applications, such as regulation of gene expression, site-specific cleavage of duplex DNA, mapping of genomic DNA, and gene-targeted mutagenesis (1–3). A triplex is usually formed through the sequence-specific interaction of a single-stranded homopurine or homopyrimidine triplex-forming oligonucleotide (TFO)[1] with the major groove of homopurine-homopyrimidine stretch in duplex DNA (1–5). In the pyrimidine motif triplex, a homopyrimidine TFO binds parallel to the homopurine strand of the target duplex by Hoogsteen hydrogen bonding to form T·A:T and C^+·G:C triplets (1–5). On the other hand, in the purine motif triplex, a homopurine TFO binds antiparallel to the homopurine strand of the target duplex by reverse Hoogsteen hydrogen bonding to form A·A:T (or T·A:T) and G·G:C triplets (1–5).

Because the cytosine bases in a homopyrimidine TFO must be protonated to bind with the guanine bases of the G:C duplex, the formation of the pyrimidine motif triplex needs an acidic pH condition and is thus extremely unstable at physiological pH (6–8). Instead, the pH-independent formation of the purine motif triplex is available at physiological pH. However, the purine motif triplex formation is severely inhibited by physiological concentrations of certain monovalent cations, especially K^+. Undefined association between K^+ and the guanine-rich homopurine TFO has been applied to explain the inhibitory effect (9, 10). Therefore, stabilization of the pyrimidine motif triplex at physiological pH is of great importance in improving its therapeutic potential to artificially control gene expression *in vivo*. Numerous efforts such as the replacement of cytosine bases in a homopyrimidine TFO with 5-methylcytosine (7, 11–13) or other chemically modified bases (14–18), the conjugation of different DNA intercalators to TFO (19, 20), and the use of polyamines such as spermine or spermidine as triplex stabilizers (21) have been made to improve the stability of the pyrimidine motif triplex at physiological pH.

We first synthesized and developed a new class of chemical modifications of nucleic acids, bridged nucleic acid (BNA), such as 2′-*O*,4′-*C*-methylene BNA (2′,4′-BNA; Fig. 1*a*; Refs. 22–27)[2] and 3′-*O*,4′-*C*-methylene BNA (3′,4′-BNA; Refs. 30–32). The 2′,4′-BNA modification of TFO increased the thermal stability of the pyrimidine motif triplex DNA at neutral pH using a homopurine-homopyrimidine target duplex and its specific cytosine-rich TFO (25). However, the mechanistic explanation for the 2′,4′-BNA modification-mediated triplex stabilization was not clearly understood. Here, therefore, we have further ex-

* This research was supported in part by Ministry of Education, Science, Sports, and Culture of Japan Grants-in Aid 08249247 and 12217158 (to H. T.) and 09557201 and 12217081 (to T. I.). The costs of publication of this article were defrayed in part by the payment of page charges. This article must therefore be hereby marked "*advertisement*" in accordance with 18 U.S.C. Section 1734 solely to indicate this fact.

§ To whom correspondence should be addressed: Tsukuba Life Science Center, Institute of Physical and Chemical Research (RIKEN), 3-1-1 Koyadai, Tsukuba, Ibaraki 305-0074, Japan. Tel.: 81-298-36-9082; Fax: 81-298-36-9080; E-mail: torigoe@rtc.riken.go.jp.

‖ To whom correspondence should be addressed: Graduate School of Pharmaceutical Sciences, Osaka University, 1-6 Yamadaoka, Suita, Osaka 565-0871, Japan. Tel.: 81-6-6879-8200; Fax: 81-6-6879-8204; E-mail: imanishi@phs.osaka-u.ac.jp.

[1] The abbreviations used are: TFO, triplex-forming oligonucleotide; BNA, bridged nucleic acid; 2′,4′-BNA, 2′-*O*,4′-*C*-methylene bridged nucleic acid; 3′,4′-BNA, 3′-*O*,4′-*C*-methylene bridged nucleic acid; EMSA, electrophoretic mobility shift assay; CD, circular dichroism; ITC, isothermal titration calorimetry; IAsys, interaction analysis system; Pur, purine; Pyr, pyrimidine; Bt, biotinylated; NS, nonspecific; T_m, melting temperature; k_{on}, on-rate constant; k_{assoc}, association rate constant; k_{off}, off-rate constant; k_{dissoc}, dissociation rate constant.

[2] After our report on the first synthesis of 2′,4′-BNA monomers, Wengel's group demonstrated some properties of 2′,4′-BNA (28, 29).

tended our previous study to explore thermodynamic and kinetic effects of the 2′,4′-BNA modification on the pyrimidine motif triplex formation at neutral pH. The thermodynamic and kinetic effects of the 2′,4′-BNA modification on the pyrimidine motif triplex formation between a 23-base pair homopurine-homopyrimidine target duplex (Pur23A·Pyr23T; Fig. 1*b*) and its specific 15-mer unmodified or 2′,4′-BNA-modified homopyrimidine TFO (Pyr15T, Pyr15BNA7-1, Pyr15BNA7-2, Pyr15BNA5-1, and Pyr15BNA5-2; Fig. 1*b*) have been analyzed by electrophoretic mobility shift assay (EMSA; Refs. 33, 34), UV melting, isothermal titration calorimetry (ITC; Refs. 34–40), and interaction analysis system (IAsys; Refs. 34, 39–43). Results from these independent lines of experiments have clearly indicated the significant effect of the 2′,4′-BNA modification to promote the pyrimidine motif triplex formation at neutral pH. The binding constant at neutral pH for the pyrimidine motif triplex formation with the 2′,4′-BNA-modified TFO was ~10–20 times larger than that observed with the corresponding unmodified TFO. Kinetic data have also demonstrated that the contribution for the increase in the binding constant by the 2′,4′-BNA modification of TFO resulted from the considerable decrease in the dissociation rate constant. The ability of the 2′,4′-BNA modification of TFO to promote the pyrimidine motif triplex formation at physiological pH would support further progress in therapeutic applications of the antigene strategy *in vivo*.

MATERIALS AND METHODS

Preparation of Oligonucleotides—We synthesized 23-mer complementary oligonucleotides for the target duplex Pur23A and Pyr23T (Fig. 1*b*), a 15-mer unmodified homopyrimidine TFO specific for the target duplex Pyr15T (Fig. 1*b*), and a nonspecific homopyrimidine oligonucleotide, Pyr15NS (Fig. 1*b*), on an Applied Biosystems DNA synthesizer using the solid-phase cyanoethyl phosphoramidite method and purified them with a reverse-phase high performance chromatography on a Wakosil DNA column. The 15-mer 2′,4′-BNA-modified homopyrimidine TFOs Pyr15BNA7-1, Pyr15BNA7-2, Pyr15BNA5-1, and Pyr15BNA5-2 (Fig. 1*b*) were synthesized and purified as described previously (22, 28). 5′ biotinylated Pyr23T (denoted Bt-Pyr23T) was prepared using biotin phosphoramidite. The concentration of all oligonucleotides was determined by UV absorbance. Complementary strands Pur23A and Pyr23T were annealed by heating at up to 90 °C, followed by a gradual cooling to room temperature. The annealed sample was applied on a hydroxyapatite column (Koken Inc.) to remove unpaired single strands. The concentration of the duplex DNA (Pur23A·Pyr23T) was determined by UV absorption considering the DNA concentration ratio of 1 optical density unit = 50 μg/ml, with an M_r of 15180.

EMSA—EMSA experiments were performed essentially as described previously (34). In 9 μl of reaction mixture, ^{32}P-labeled duplex (~1 ng) was mixed with increasing concentrations of the specific TFO (Pyr15T, Pyr15BNA7-1, Pyr15BNA7-2, Pyr15BNA5-1, or Pyr15BNA5-2) and the nonspecific oligonucleotide (Pyr15NS) in a buffer containing 50 mM Tris acetate, pH 7.0, 100 mM sodium chloride, and 10 mM magnesium chloride. Pyr15NS was added to achieve equimolar concentrations of TFO in each lane as well as to minimize adhesion of the DNA (target duplex and TFO) to plastic surfaces during incubation and subsequent losses during processing. After 6 h of incubation at 37 °C, 2 μl of 50% glycerol solution containing bromphenol blue was added without changing the pH and salt concentrations of the reaction mixtures. Samples were then directly loaded onto a 15% native polyacrylamide gel prepared in buffer (50 mM Tris acetate, pH 7.0, and 10 mM magnesium chloride), and electrophoresis was performed at 8 V/cm for 16 h at 4 °C.

UV Melting—UV melting experiments were carried out on a Jasco Ubest-30 spectrophotometer equipped with an EHC-363 Peltier-type cell holder controlled by a TPU-436 temperature programmer. UV melting profiles were measured in buffer A (10 mM sodium cacodylate-cacodylic acid, pH 6.8, containing 200 mM NaCl and 20 mM $MgCl_2$) at a scan rate of 0.5 °C/min at 260 nm. The first derivative was calculated from the UV melting profile. The peak temperatures in the derivative curve were designated the melting temperatures (T_ms). Cell path length was 1 cm. The triplex DNA concentration used was 1 μM.

Circular Dichroism (CD) Spectroscopy—CD spectra at room temperature were recorded in buffer A on a Jasco J-720 spectropolarimeter interfaced with a microcomputer. Cell path length was 1 cm. The triplex DNA concentration used was 4 μM.

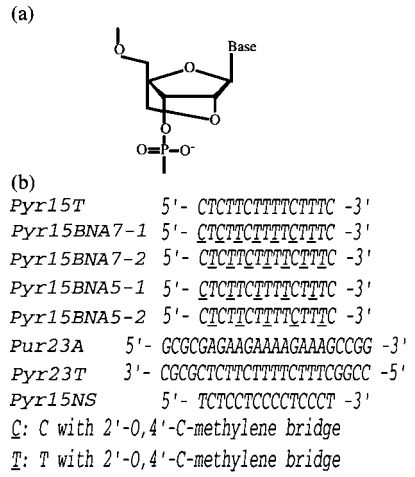

FIG. 1. ***a*, nucleotide unit of 2′,4′-BNA. *b*, oligonucleotide sequences of the target duplex (Pur23A·Pyr23T), the specific TFOs (Pyr15T, Pyr15BNA7-1, Pyr15BNA7-2, Pyr15BNA5-1, and Pyr15BNA5-2), and the nonspecific oligonucleotide (Pyr15NS).**

ITC—Isothermal titration experiments were carried out on an MCS ITC system (Microcal Inc.), essentially as described previously (34, 38, 39). The TFO and Pur23A·Pyr23T duplex DNA solutions were prepared by extensive dialysis against buffer A or buffer B (10 mM sodium cacodylate-cacodylic acid, pH 5.8, containing 200 mM NaCl and 20 mM $MgCl_2$). The TFO solution in buffer A or buffer B was injected 20 times in 5-μl increments and 10-min intervals into the Pur23A·Pyr23T duplex solution without changing the reaction conditions. The heat for each injection was subtracted by the heat of dilution of the injectant, which was measured by injecting the TFO into the same buffer. Each corrected heat was divided by the moles of the TFO injected and analyzed with Microcal Origin software supplied by the manufacturer.

IAsys—Kinetic experiments by resonant mirror method were performed on an IAsys Plus instrument (Affinity Sensors Cambridge Inc.), essentially as described previously, in which a real-time biomolecular interaction was measured with a laser biosensor (34, 39). The resonant layer of a cuvette was washed with 80 μl of 10 mM acetate buffer, pH 4.6, and then activated with 80 μl of a mixture of 1-ethyl-3-(3-dimethylaminopropyl) carbodiimide and *N*-hydroxysuccinimide solution. The activated surface was again washed with 10 mM acetate buffer, pH 4.6, and streptavidin in 10 mM acetate buffer, pH 4.6, was immobilized to the surface. After blocking the remaining reactive groups with 1 M ethanolamine, pH 8.5, the cuvette was extensively washed with 10 mM acetate buffer, pH 4.6, and then with 20 mM HCl to remove the loosely associated protein. The cuvette was washed with buffer A, and Bt-Pyr23T (1.2 μM in buffer A) was added to bind with the streptavidin on the surface. After washing the cuvette with the same buffer, the complementary oligonucleotide Pur23A (1.2 μM in buffer A) was added to hybridize with Bt-Pyr23T. After extensive washing and equilibrating the Bt-Pyr23T·Pur23A-immobilized surface with buffer A for >30 min, the TFO in 80 μl of buffer A was injected over the immobilized Bt-Pyr23T·Pur23A duplex, and then the triplex formation was monitored for 30 min. This was followed by washing the cuvette with buffer A, and the dissociation of the preformed triplex was monitored for an additional 20 min. Finally, 10 mM NaOH, pH 12, was injected for 3 min for complete break of the Hoogsteen hydrogen bonding between the TFO and Pur23A, during which the Bt-Pyr23T·Pur23A duplex may be partially denatured. The Bt-Pyr23T·Pur23A duplex was regenerated by injecting 1.2 μM Pur23A. The resulting sensorgrams were analyzed with Fastfit software supplied by the manufacturer to calculate the kinetic parameters.

RESULTS

Electrophoretic Mobility Shift Assay of Pyrimidine Motif Triplex Formation at Neutral pH—The pyrimidine motif triplex formation of the target duplex (Pur23A·Pyr23T; Fig. 1*b*) with unmodified (Pyr15T; Fig. 1*b*) or 2′,4′-BNA-modified (Pyr15BNA7-1, Pyr15BNA7-2, Pyr15BNA5-1, or Pyr15BNA5-2; Fig. 1*b*) TFO was examined at pH 7.0 by EMSA (Fig. 2). The total oligonucleotide concentration ([specific TFO (Pyr15T, Pyr15BNA7-1, Pyr15BNA7-2, Pyr15BNA5-1, or Pyr15BNA5-2; Fig. 1*b*)] + [non-

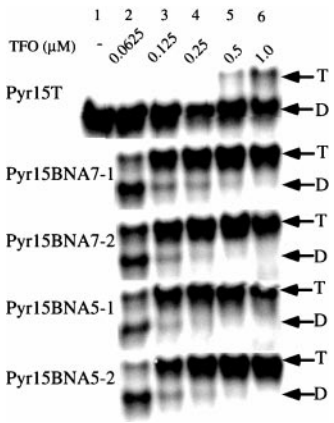

FIG. 2. **EMSA of the pyrimidine motif triplex formation with the specific TFO (Pyr15T, Pyr15BNA7-1, Pyr15BNA7-2, Pyr15BNA5-1, or Pyr15BNA5-2) at neutral pH.** Triplex formation was initiated by adding ^{32}P-labeled Pur23A·Pyr23T duplex (~1 ng) with the indicated final concentrations of the specific TFO (Pyr15T, Pyr15BNA7-1, Pyr15BNA7-2, Pyr15BNA5-1, or Pyr15BNA5-2). The nonspecific oligonucleotide (Pyr15NS) was added to adjust the equimolar concentrations of TFO (1 μM) in each lane. The reaction mixtures in the buffer (50 mM Tris acetate, pH 7.0, 100 mM sodium chloride, and 10 mM magnesium chloride) were incubated for 6 h at 37 °C, and then electrophoretically separated on a 15% native polyacrylamide gel at 4 °C. The positions of the duplex (*D*) and triplex (*T*) are indicated.

specific oligonucleotide (Pyr15NS; Fig. 1*b*)]) was kept constant at 1 μM to minimize loss of DNA during processing. Although incubation with 1 μM Pyr15NS alone did not cause a shift in electrophoretic migration of the target duplex (see Fig. 2, *lane 1* for Pyr15T), those with Pyr15T, Pyr15BNA7-1, Pyr15BNA7-2, Pyr15BNA5-1, or Pyr15BNA5-2 at particular concentration caused retardation of the duplex migration owing to triplex formation (33). The K_d of triplex formation was determined from the concentration of the TFO, which caused half of the target duplex to shift to the triplex (33). The K_d of the triplex with Pyr15T was estimated to be ~1.0 μM. In contrast, the K_d of the triplex with Pyr15BNA7-1, Pyr15BNA7-2, Pyr15BNA5-1, or Pyr15BNA5-2 was ~0.06 μM, indicating that the 2′,4′-BNA modification of TFO increased the binding affinity of the pyrimidine motif triplex formation at neutral pH by ~20 times. The increase in the K_a by the 2′,4′-BNA modification was similar in magnitude among the four modified TFOs.

Spectroscopic Characterization of Pyrimidine Motif Triplex at Neutral pH—The thermal stability of the pyrimidine motif triplex with unmodified (Pyr15T) or 2′,4′-BNA-modified (Pyr15BNA7-1, Pyr15BNA7-2, Pyr15BNA5-1, or Pyr15BNA5-2) TFO was investigated at pH 6.8 by UV melting (Fig. 3 and Table I). All the triplexes showed two-step melting. The first transition at a lower temperature, T_{m1}, was the melting of the triplex to a duplex and a TFO, and the second transition at a higher temperature, T_{m2}, was the melting of the duplex (Fig. 3). Although the T_{m2} was almost identical among all the triplexes, the T_{m1} for Pyr15BNA7-1, Pyr15BNA7-2, Pyr15BNA5-1, or Pyr15BNA5-2 was significantly higher than that for Pyr15T (Table I), indicating that the 2′,4′-BNA modification of TFO increased the thermal stability of the pyrimidine motif triplex at neutral pH.

To further characterize the triplexes involving unmodified (Pyr15T) or 2′,4′-BNA-modified (Pyr15BNA7-1, Pyr15BNA7-2, Pyr15BNA5-1, or Pyr15BNA5–2) TFO, CD spectra of the triplexes were measured at 25 °C and pH 6.8 (Fig. 4). The overall shape of the CD spectra was similar among all the profiles. A negative band in the short-wavelength (210–220-nm) region was observed for all the profiles, confirming the triplex formation involving each TFO (44, 45). The intensity of the negative short-wavelength (210–220-nm) band for the triplexes

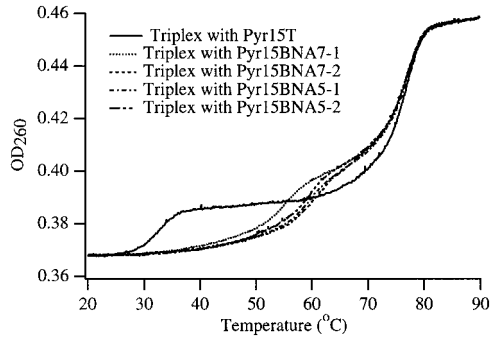

FIG. 3. **UV melting profiles of the pyrimidine motif triplex with the specific TFO (Pyr15T, Pyr15BNA7-1, Pyr15BNA7-2, Pyr15BNA5-1, or Pyr15BNA5-2) at neutral pH.** The triplexes in buffer A were melted at a scan rate of 0.5 °C/min with detection at 260 nm. Cell path length was 1 cm. The triplex DNA concentration used was 1 μM.

TABLE I

Melting temperatures of the triplexes between a 15-mer TFO (Pyr15T, Pyr15BNA7–1, Pyr15BNA7–2, Pyr15BNA5–1, or Pyr15BNA5–2) and a 23 base pair target duplex (Pur23A · Pyr23T)

Melting temperatures were at pH 6.8 in 10 mM sodium cacodylate-cacodylic acid, 200 mM sodium chloride, and 20 mM magnesium chloride, obtained from UV melting.

TFO	T_{m1}	T_{m2}
	°C	°C
Pyr15T	33.2	77.1
Pyr15BNA7–1	55.6	77.0
Pyr15BNA7–2	61.0	76.9
Pyr15BNA5–1	60.1	77.0
Pyr15BNA5–2	60.0	77.0

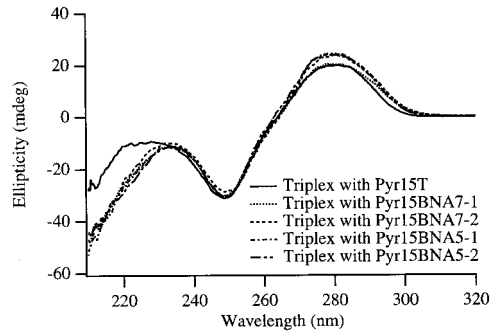

FIG. 4. **CD spectra of the pyrimidine motif triplex with the specific TFO (Pyr15T, Pyr15BNA7-1, Pyr15BNA7-2, Pyr15BNA5-1, or Pyr15BNA5-2) at neutral pH.** The triplexes at 25 °C and pH 6.8 in buffer A were measured in the wavelength range of 210–320 nm. Cell path length was 1 cm. The triplex DNA concentration used was 4 μM.

involving Pyr15BNA7-1, Pyr15BNA7-2, Pyr15BNA5-1, or Pyr15BNA5-2 was larger than that observed for the triplex involving Pyr15T, indicating that all the pyrimidine motif triplexes involving the 2′,4′-BNA-modified TFO had more aspects of the A conformation than that involving the unmodified TFO (45).

Thermodynamic Analyses of Pyrimidine Motif Triplex Formation at Neutral pH by ITC—We examined the thermodynamic parameters of the pyrimidine motif triplex formation between a 23-base pair target duplex (Pur23A·Pyr23T) and its specific 15-mer unmodified (Pyr15T) or 2′,4′-BNA-modified (Pyr15BNA7-1, Pyr15BNA7-2, Pyr15BNA5-1, or Pyr15BNA5-2) TFO at 25 °C and pH 6.8 by ITC. To investigate the pH dependence of the pyrimidine motif triplex formation, the thermodynamic parameters of the triplex formation between Pur23A·Pyr23T and Pyr15T were also analyzed at 25 °C and pH 5.8 by ITC. Fig. 5a compares the ITC profiles of the initial

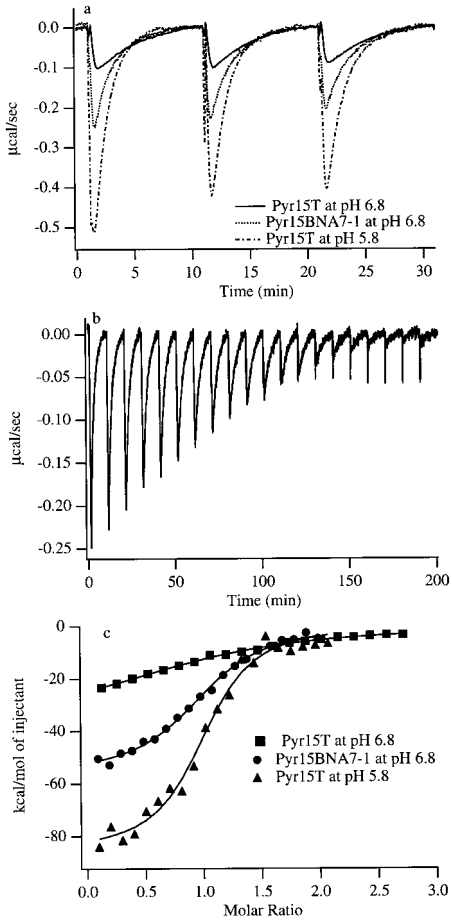

FIG. 5. **Thermodynamic analyses of the pyrimidine motif triplex formation with Pyr15T or Pyr15BNA7-1 at pH 6.8 and with Pyr15T at pH 5.8 by ITC.** *a*, ITC profiles of the initial three injections for the binding of Pur23A·Pyr23T to Pyr15T or Pyr15BNA7-1 at 25 °C and pH 6.8 and to Pyr15T at 25 °C and pH 5.8. The TFO solution (120 μM in buffer A or buffer B; see "Materials and Methods") was injected in 5-μl increments into 5 μM Pur23A·Pyr23T solution in the same buffer. Injections occurred over 10 s at 10-min intervals. *b*, total ITC profile for the triplex formation between Pyr15BNA7-1 and Pur23A·Pyr23T. The Pyr15BNA7-1 solution was injected 20 times into the Pur23A·Pyr23T solution. Other experimental conditions were the same as in *a*. *c*, titration plots against the molar ratio of [TFO]/[Pur23A·Pyr23T]. The data were fitted by a nonlinear least squares method.

three injections for the binding of Pur23A·Pyr23T with Pyr15T or Pyr15BNA7-1 at pH 6.8 and with Pyr15T at pH 5.8. The magnitudes of the exothermic peaks for Pyr15BNA7-1 at pH 6.8 and for Pyr15T at pH 5.8 were larger than those observed for Pyr15T at pH 6.8. Fig. 5b shows an ITC profile over 200 min for triplex formation with Pyr15BNA7-1 at pH 6.8. An exothermic heat pulse was observed after each injection of Pyr15BNA7-1 into Pur23A·Pyr23T. The magnitude of each peak decreased gradually with each new injection, and a small peak was still observed at a molar ratio of [Pyr15BNA7-1]/[Pur23A·Pyr23T] = 2. The area of the small peak was equal to the heat of dilution measured in a separate experiment by injecting Pyr15BNA7-1 into the same buffer (data not shown). The area under each peak was integrated, and the heat of dilution of Pyr15BNA7-1 was subtracted from the integrated values. The corrected heat was divided by the moles of injected solution, and the resulting values were plotted as a function of a molar ratio of [Pyr15BNA7-1]/[Pur23A·Pyr23T], as shown in Fig. 5*c*. The resultant titration plot was fitted to a sigmoidal curve by a nonlinear least-squares method. The binding constant, K_a, and the enthalpy change, ΔH, were obtained from the fitted curve (37). The Gibbs free energy change, ΔG, and the entropy change, ΔS, were calculated from the equation, $\Delta G = -RT\ln K_a = \Delta H - T\Delta S$ (37) where R is gas constant and T is temperature. The titration plots for Pyr15T at pH 5.8 and pH 6.8 are also shown in Fig. 5*c*. The thermodynamic parameters for Pyr15T at pH 5.8 and 6.8 were obtained from the titration plots in the same way. The ITC profiles and the titration plots for Pyr15BNA7-2, Pyr15BNA5-1, and Pyr15BNA5-2 at pH 6.8 were almost the same as those observed for Pyr15BNA7-1 at pH 6.8 (data not shown). The thermodynamic parameters for Pyr15BNA7-2, Pyr15BNA5-1, and Pyr15BNA5-2 at pH 6.8 were obtained in the same way.

Table II summarizes the thermodynamic parameters for the pyrimidine motif triplex formation with all the TFOs at 25 °C and pH 6.8 and those with Pyr15T at 25 °C and pH 5.8, obtained from ITC. The signs of both ΔH and ΔS were negative under all the conditions. Because an observed negative ΔS was unfavorable for the triplex formation, the triplex formation was driven by a large negative ΔH under each condition. The magnitudes of the negative ΔH of the triplex formation for Pyr15T at pH 5.8 and for Pyr15BNA7-1, Pyr15BNA7-2, Pyr15BNA5-1, or Pyr15BNA5-2 at pH 6.8 were 2.5 or 1.6–1.7 times larger than that observed for Pyr15T at pH 6.8, consistent with the ITC profiles in Fig. 5*a*. The K_a for Pyr15T at pH 5.8 was ~20 times larger than that observed for Pyr15T at pH 6.8, confirming, like others (6–8), that neutral pH is unfavorable for the pyrimidine motif triplex formation involving C^+·G:C triads. In addition, the K_a for Pyr15BNA7-1, Pyr15BNA7-2, Pyr15BNA5-1, or Pyr15BNA5-2 at pH 6.8 was 10–20 times larger than that observed for Pyr15T at pH 6.8, indicating that the 2′,4′-BNA modification of TFO increased the K_a of the pyrimidine motif triplex formation at neutral pH by 10–20 times. The increase in the K_a by the 2′,4′-BNA modification of TFO was similar in magnitude among the four modified TFOs.

Kinetic Analyses of Pyrimidine Motif Triplex Formation at Neutral pH by IAsys—To examine the putative mechanism involved in the increase in K_a of the pyrimidine motif triplex formation by the 2′,4′-BNA modification (Fig. 2 and Table II), we assessed the kinetic parameters for the association and dissociation of TFO (Pyr15T, Pyr15BNA7-1, Pyr15BNA7-2, Pyr15BNA5-1, or Pyr15BNA5-2) with Pur23A·Pyr23T at 25 °C and pH 6.8 by IAsys. Fig. 6*a* compares the sensorgrams representing the triplex formation and dissociation involving 90 μM of the specific TFO (Pyr15T or Pyr15BNA7-1). The injection of Pyr15T over the immobilized Bt-Pyr23T·Pur23A caused an increase in response. The response was substantially delayed on the injection of Pyr15BNA7-1, indicating that the 2′,4′-BNA modification decreased the association rate constant of the triplex equilibrium. In contrast, the change in the dissociation curve with time for Pyr15BNA7-1 was much smaller than that for Pyr15T. The result clearly indicated that the 2′,4′-BNA modification of TFO remarkably decreased the dissociation rate constant of the triplex equilibrium. The similar profiles were obtained for Pyr15BNA7-2, Pyr15BNA5-1, and Pyr15BNA5-2.

To understand the kinetic parameters more quantitatively, we analyzed a series of association and dissociation curves at the various concentrations of TFO. As shown in Fig. 6*b*, an increase in the concentration of the 2′,4′-BNA-modified TFO (Pyr15BNA7-1) led to a gradual change in the response of the association curves. The k_{on} was obtained from the analysis of each association curve. Fig. 6*c* shows a plot of k_{on} against the Pyr15BNA7-1 concentrations. The resultant plot was fitted to a straight line by a linear least-squares method. The association rate constant (k_{assoc}) and the dissociation rate constant (k_{dissoc}) were determined from the slope and the intercept of the regression line, respectively (41–43). The kinetic parameters for the triplex formation with Pyr15BNA7-2, Pyr15BNA5-1, and

TABLE II
Thermodynamic parameters for the triplex formation between a 15-mer TFO (Pyr15T, Pyr15BNA7–1, Pyr15BNA7–2, Pyr15BNA5–1, or Pyr15BNA5–2) and a 23-base pair duplex (Pur23A · Pyr23T) at 25 °C, obtained from ITC

TFO	pH	K_a	K_a (relative)	ΔG	ΔH	ΔS
		/M		kcal/mol	kcal/mol	cal/mol/K
Pyr15T	5.8[a]	$(3.83 \pm 0.74) \times 10^6$	19.4	-8.98 ± 0.13	-85.6 ± 2.6	-257 ± 9.1
Pyr15T	6.8[b]	$(1.97 \pm 0.43) \times 10^5$	1.0	-7.22 ± 0.15	-34.9 ± 2.2	-92.7 ± 8.0
Pyr15BNA7–1	6.8[b]	$(2.28 \pm 0.32) \times 10^6$	11.6	-8.67 ± 0.09	-55.5 ± 1.5	-157 ± 5.3
Pyr15BNA7–2	6.8[b]	$(2.16 \pm 0.38) \times 10^6$	11.0	-8.64 ± 0.11	-57.3 ± 2.0	-163 ± 7.2
Pyr15BNA5–1	6.8[b]	$(3.65 \pm 0.54) \times 10^6$	18.5	-8.95 ± 0.10	-60.7 ± 1.4	-174 ± 5.1
Pyr15BNA5–2	6.8[b]	$(2.06 \pm 0.42) \times 10^6$	10.5	-8.61 ± 0.14	-60.5 ± 2.6	-174 ± 9.2

[a] 10 mM sodium cacodylate-cacodylic acid, pH 5.8, 200 mM sodium chloride, and 20 mM magnesium chloride.
[b] 10 mM sodium cacodylate-cacodylic acid, pH 6.8, 200 mM sodium chloride, and 20 mM magnesium chloride.

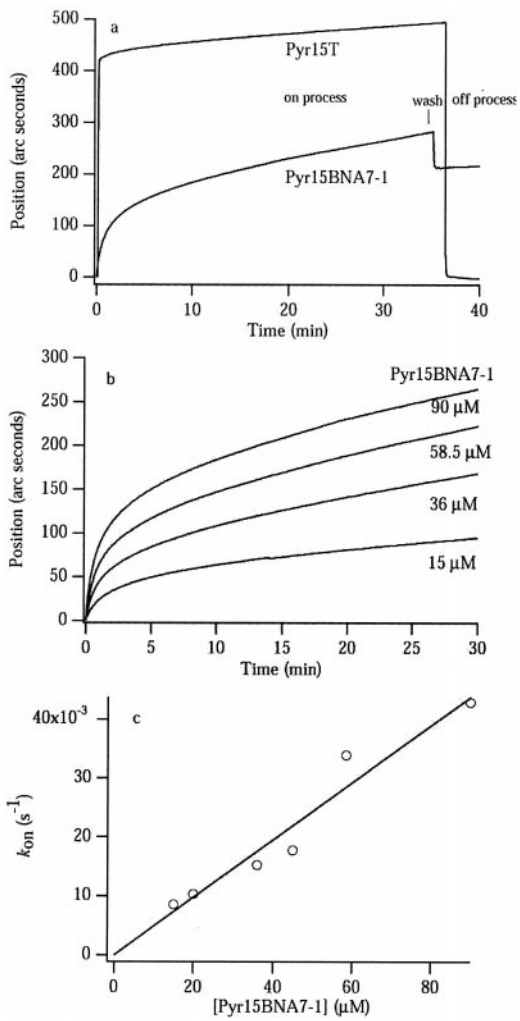

FIG. 6. **Kinetic analyses of the pyrimidine motif triplex formation with Pyr15T or Pyr15BNA7-1 at pH 6.8 by IAsys.** *a*, typical sensorgrams for the triplex formation at 25 °C and pH 6.8 after injecting 90 μM specific TFO (Pyr15T or Pyr15BNA7-1) in buffer A into the Bt-Pyr23T·Pur23A-immobilized cuvette. *b*, series of sensorgrams for the triplex formation between Pyr15BNA7-1 and Pur23A·Pyr23T at 25 °C and pH 6.8. The Pyr15BNA7-1 solution, diluted in buffer A to achieve the indicated final concentrations, was injected into the Bt-Pyr23T·Pur23A-immobilized cuvette. The binding of Pyr15BNA7-1 to Bt-Pyr23T·Pur23A was monitored as the response against time. *c*, measured k_{on} values of the triplex formation in *b* were plotted against the respective concentrations of Pyr15BNA7-1. The plot was fitted to a straight line ($r^2 = 0.97$) by a linear least squares method.

Pyr15BNA5-2 were obtained in the same way. K_a was calculated from the equation, $K_a = k_{assoc}/k_{dissoc}$. Because the change of the dissociation curves with time was very small for Pyr15BNA7-1, Pyr15BNA7-2, Pyr15BNA5-1, and Pyr15BNA5-2 (Fig. 6*a*; data not shown), that is, the dissociation was very slow, we could not directly determine the k_{dissoc} from the dissociation curves. Thus, the k_{dissoc} obtained from the association curves was presented for Pyr15BNA7-1, Pyr15BNA7-2, Pyr15BNA5-1, and Pyr15BNA5-2, although its S.D. was relatively large (Table III). On the other hand, although the k_{assoc} for Pyr15T was obtained in the same way as described above, the k_{dissoc} for Pyr15T was determined in the following way owing to the much faster dissociation. The off-rate constant (k_{off}) was obtained from the analysis of each dissociation curve (Fig. 6*a*; data not shown). Because k_{off} is usually independent of the concentration of the injected solution, the k_{dissoc} was determined by averaging k_{off} for several concentrations (41–43). K_a was calculated from the equation $K_a = k_{assoc}/k_{dissoc}$.

Table III summarizes the kinetic parameters for the pyrimidine motif triplex formation with all the TFOs at 25 °C and pH 6.8, obtained from IAsys. The magnitudes of K_a calculated from the ratio of k_{assoc} to k_{dissoc} (Table III) were consistent with those obtained from ITC (Table II). The 2′,4′-BNA modification of TFO increased the K_a for the pyrimidine motif triplex formation at neutral pH, which supported the results of EMSA (Fig. 2) and ITC (Table II). The k_{dissoc} of the triplex formation decreased ~40–70 times by the 2′,4′-BNA modification of TFO. In contrast, when the k_{assoc} of the triplex formation was compared, 1–1.3 times smaller k_{assoc} was obtained by the 2′,4′-BNA modification of TFO, which opposes the increase in K_a. Thus, the much larger K_a by the 2′,4′-BNA modification resulted from the decrease in k_{dissoc}. The kinetic effect to increase the K_a by the 2′,4′-BNA modification was similar among the four modified TFOs.

DISCUSSION

The K_a of the pyrimidine motif triplex formation with Pyr15T at pH 5.8 was 20 times larger than that observed with Pyr15T at pH 6.8 (Table II), which is consistent with the previously reported results that the neutral pH is unfavorable for the pyrimidine motif triplex formation involving C^+·GC triads (6–8). The K_a of the triplex formation with Pyr15BNA7-1, Pyr15BNA7-2, Pyr15BNA5-1, or Pyr15BNA5-2 at pH 6.8 was 10–20 times larger than that observed with Pyr15T at pH 6.8 (Table II). The increase in K_a at pH 6.8 by the 2′,4′-BNA modification of TFO was supported by the results of EMSA (Fig. 2) and IAsys (Table III). In addition, the 2′,4′-BNA modification of TFO increased the thermal stability of the pyrimidine motif triplex at pH 6.8 (Table I). These results indicate that the 2′,4′-BNA modification of TFO considerably promotes the pyrimidine motif triplex formation at neutral pH.

The ΔH on the triplex formation measured by ITC reflects a major contribution from the hydrogen bonding and the base stacking involved in the triplex formation (38, 46–48). On the other hand, the ΔS on the triplex formation measured by ITC includes a positive entropy change from release of structured water on the triplex formation and a major contribution of a

TABLE III

Kinetic parameters for the triplex formation between a 15-mer TFO (Pyr15T, Pyr15BNA7–1, Pyr15BNA7–2, Pyr15BNA5–1, or Pyr15BNA5–2) and a 23-base pair duplex (Pur23A · Pyr23T)

Parameters were at 25 °C and pH 6.8 in 10 mM sodium cacodylate-cacodylic acid, 200 mM sodium chloride, and 20 mM magnesium chloride, obtained from IAsys.

TFO	k_{assoc}	k_{assoc} (relative)	k_{dissoc}	k_{dissoc} (relative)	K_a	K_a (relative)
	$/M/s$		$/s$		$/M$	
Pyr15T	$(6.31 \pm 0.18) \times 10^2$	1.0	$(1.17 \pm 0.14) \times 10^{-2}$	1.0	$(5.41 \pm 0.91) \times 10^4$	1.0
Pyr15BNA7–1	$(4.86 \pm 0.60) \times 10^2$	0.77	$(1.57 \pm 3.04) \times 10^{-4}$	0.013	$(3.09 \pm 0.38) \times 10^6$	57.1
Pyr15BNA7–2	$(5.05 \pm 0.77) \times 10^2$	0.80	$(2.35 \pm 3.07) \times 10^{-4}$	0.020	$(2.15 \pm 1.36) \times 10^6$	39.7
Pyr15BNA5–1	$(5.93 \pm 0.93) \times 10^2$	0.94	$(2.97 \pm 2.06) \times 10^{-4}$	0.025	$(2.00 \pm 1.02) \times 10^6$	37.0
Pyr15BNA5–2	$(6.32 \pm 0.34) \times 10^2$	1.0	$(2.66 \pm 1.67) \times 10^{-4}$	0.023	$(2.38 \pm 1.00) \times 10^6$	44.0

negative conformational entropy change from the conformational restraint of TFO involved in the triplex formation (38, 46–48). Because the formed triplex structure involving Pyr15T at pH 5.8 and that involving Pyr15T at pH 6.8 is the same, the magnitude of ΔH and ΔS on the triplex formation measured by ITC could be the same between the two conditions. However, unexpectedly, the magnitudes of ΔH and ΔS for Pyr15T at pH 6.8 were significantly smaller than those observed for Pyr15T at pH 5.8 (Table II). When the ΔH and ΔS are calculated from the fitting procedure of ITC, the heat observed by ITC is divided not by the effective concentration really involved in the triplex formation but by the apparent concentration added to the triplex formation (37). The calculation does not take it into consideration what percentage of the added concentration is really effectively involved in the triplex formation. Thus, if the triplex formation is less stoichiometric under a certain condition, the magnitudes of ΔH and ΔS for the less stoichiometric triplex formation estimated by ITC are smaller than those observed for the more stoichiometric triplex formation under another condition. Therefore, the significantly smaller magnitudes of ΔH and ΔS for Pyr15T at pH 6.8 relative to those for Pyr15T at pH 5.8 (Table II) suggest that the triplex formation with Pyr15T at pH 6.8 was significantly less stoichiometric than that with Pyr15T at pH 5.8, which was also supported by the significantly smaller magnitudes of K_a and ΔG for Pyr15T at pH 6.8 (Table II). In contrast, the K_a and ΔG for Pyr15T at pH 5.8 and those for the 2′,4′-BNA modified TFOs at pH 6.8 were quite similar (Table II), suggesting that the triplex formation under the two conditions was similarly quite stoichiometric. We conclude that the triplex formation with Pyr15T at pH 6.8 was significantly less stoichiometric than that with Pyr15T at pH 5.8 and that with the 2′,4′-BNA-modified TFOs at pH 6.8. Thus, to discuss the promotion mechanism of the triplex formation by the 2′,4′-BNA modification, the comparison of the ΔH and ΔS between Pyr15T at pH 6.8 and 2′,4′-BNA-modified TFOs at pH 6.8 is not valid because of the significantly reduced stoichiometry for Pyr15T at pH 6.8. The comparison of the ΔH and ΔS between Pyr15T at pH 5.8 and 2′,4′-BNA-modified TFOs at pH 6.8 with similar stoichiometry will provide a reasonable promotion mechanism for the triplex formation by the 2′,4′-BNA modification, as discussed below.

Although the K_a and ΔG for Pyr15T at pH 5.8 and those for the 2′,4′-BNA-modified TFOs at pH 6.8 were quite similar (Table II), the ingredients of ΔG, that is, ΔH and ΔS, were obviously different from each other. The magnitudes of the negative ΔH and ΔS for the 2′,4′-BNA-modified TFOs at pH 6.8 were smaller than those observed for Pyr15T at pH 5.8 (Table II). The hydrogen bonding and the base stacking involved in the triplex formation are usually considered the major sources of the negative ΔH on the triplex formation (38, 46–48). Thus, the difference in ΔH for the stoichiometric triplex formations between Pyr15T at pH 5.8 and the 2′,4′-BNA-modified TFOs at pH 6.8 (Table II) suggests that the hydrogen bonding and the base stacking of the triplex with the 2′,4′-BNA-modified TFOs are significantly different from those with the corresponding unmodified TFO. In fact, the CD spectra show that the triplexes with the 2′,4′-BNA-modified TFO had the A-like conformation (Ref. 45 and Fig. 4). The A-like conformation by the 2′,4′-BNA modification of TFO may result in the difference in the negative ΔH between the unmodified and 2′,4′-BNA-modified TFOs. On the other hand, the negative ΔS on the triplex formation is mainly contributed by a negative conformational entropy change attributable to the conformational restraint of TFO involved in the triplex formation (38, 46–48). Therefore, the smaller magnitude of the negative ΔS for the 2′,4′-BNA modified TFOs at pH 6.8 relative to that for Pyr15T at pH 5.8 (Table II) suggests that the 2′,4′-BNA-modified TFO in the free state is more rigid than the corresponding unmodified TFO. The increased rigidity of the 2′,4′-BNA modified TFO in the free state relative to the corresponding unmodified TFO causes the smaller entropic loss on the triplex formation with the 2′,4′-BNA-modified TFO at neutral pH, which provides a favorable component to the ΔG and leads to the increase in the K_a of the triplex formation at neutral pH. We conclude that the increased rigidity of the 2′,4′-BNA-modified TFO in the free state may be one of the factors that increases the K_a of the pyrimidine motif triplex formation at neutral pH.

The increase in the K_a by the 2′,4′-BNA modification was similar in magnitude among the four modified TFOs (Fig. 2 and Tables II and III), indicating that the number and position of the 2′,4′-BNA modification did not significantly affect the magnitude of the increase in the K_a at neutral pH. The rigidity itself of the 2′,4′-BNA-modified TFO may be more important to achieve the increase in the K_a at neutral pH than the variation of the number and position of the 2′,4′-BNA modification. Thus, other modification strategies to gain the increased rigidity of TFO may also be useful to increase the K_a at neutral pH.

Kinetic data have demonstrated that the 2′,4′-BNA modification of TFO considerably decrease the k_{dissoc} of the pyrimidine motif triplex formation (Table III). The decrease in the k_{dissoc} is a plausible kinetic reason to explain the remarkable gain in the K_a at neutral pH by the 2′,4′-BNA modification (Fig. 2 and Tables II and III). Both our group (38) and others (49) have previously proposed a model that triplexes form along nucleation-elongation processes: in a nucleation step only a few base contacts of the Hoogsteen hydrogen bonds may be formed between TFO and the target duplex, and this may be followed by an elongation step, in which Hoogsteen base pairings progress to complete triplex formation. Both groups (38, 49) have also suggested that the observed K_a, which is the ratio of k_{assoc} to k_{dissoc}, may mostly reflect rapid equilibrium of the nucleation step, which is probably the rate-limiting process of the triplex formation. In this sense, the 2′,4′-BNA modification of TFO is considered to slow the collapse of the nucleation intermediate using the rigidity of TFO to increase the K_a of the pyrimidine motif triplex formation.

The present study has clearly demonstrated that the 2′,4′-BNA modification of TFO promotes pyrimidine motif triplex formation at neutral pH. We conclude that the design of TFO to bridge different positions of sugar moiety with the alkyl chain to gain the increased rigidity of TFO is certainly a promising strategy for the promotion of triplex formation under physiological condition and may eventually lead to progress in therapeutic applications of the antigene strategy *in vivo*.

Acknowledgments—We gratefully acknowledge Dr. Hiroshi Nakanishi and Dr. Koko Mizumachi for generous consideration concerning the use of the CD spectropolarimeter and IAsys Plus instrument, respectively.

REFERENCES

1. Mirkin, S. M., and Frank-Kamenetskii, M. D. (1994) *Annu. Rev. Biophys. Biomol. Struct.* **23,** 541–576
2. Frank-Kamenetskii, M. D., and Mirkin, S. M. (1995) *Annu. Rev. Biochem.* **64,** 65–95
3. Soyfer, V. N., and Potaman, V. N. (1996) *Triple-Helical Nucleic Acids*, Springer-Verlag, New York
4. Sun, J.-S., and Helene, C. (1993) *Curr. Opin. Struct. Biol.* **3,** 345–356
5. Sun, J.-S., Garestier, T., and Helene, C. (1996) *Curr. Opin. Struct. Biol.* **6,** 327–333
6. Frank-Kamenetskii, M. D. (1992) *Methods Enzymol.* **211,** 180–191
7. Singleton, S. F., and Dervan, P. B. (1992) *Biochemistry* **31,** 10995–11003
8. Shindo, H., Torigoe, H., and Sarai, A. (1993) *Biochemistry* **32,** 8963–8969
9. Milligan, J. F., Krawczyk, S. H., Wadwani, S., and Matteucci, M. D. (1993) *Nucleic Acids Res.* **21,** 327–333
10. Cheng, A.-J., and Van Dyke, M. W. (1993) *Nucleic Acids Res.* **21,** 5630–5635
11. Lee, J. S., Woodsworth, M. L., Latimer, L. J. P., and Morgan, A. R. (1984) *Nucleic Acids Res.* **12,** 6603–6614
12. Povsic, T. J., and Dervan, P. B. (1989) *J. Am. Chem. Soc.* **111,** 3059–3061
13. Xodo, L. E., Manzini, G., Quadrifoglio, F., van der Marel, G. A., and van Boom, J. H. (1991) *Nucleic Acids Res.* **19,** 5625–5631
14. Ono, A., Ts'o, P. O. P., and Kan, L.-S. (1991) *J. Am. Chem. Soc.* **113,** 4032–4033
15. Krawczyk, S. H., Milligan, J. F., Wadwani, S., Moulds, C., Froehler, B. C., and Matteucci, M. D. (1992) *Proc. Natl. Acad. Sci. U. S. A.* **89,** 3761–3764
16. Koh, J. S., and Dervan, P. B. (1992) *J. Am. Chem. Soc.* **114,** 1470–1478
17. Jetter, M. C., and Hobbs, F. W. (1993) *Biochemistry* **32,** 3249–3254
18. Ueno, Y., Mikawa, M., and Matsuda, A. (1998) *Bioconj. Chem.* **9,** 33–39
19. Sun, J. S., Giovannangeli, C., Francois, J. C., Kurfurst, R., Montenay-Garestier, T., Asseline, U., Saison-Behmoaras, T., Thuong, N. T., and Helene, C. (1991) *Proc. Natl. Acad. Sci. U. S. A.* **88,** 6023–6027
20. Mouscadet, J.-F., Ketterle, C., Goulaouic, H., Carteau, S., Subra, F., Le Bret, M., and Auclair, C. (1994) *Biochemistry* **33,** 4187–4196
21. Hampel, K. J., Crosson, P., and Lee, J. S. (1991) *Biochemistry* **30,** 4455–4459
22. Obika, S., Nanbu, D., Hari, Y., Morio, K., In, Y., Ishida, T., and Imanishi, T. (1997) *Tetrahedron Lett.* **38,** 8735–8738
23. Obika, S., Nanbu, D., Hari, Y., Andoh, J., Morio, K., Doi, T., and Imanishi, T. (1998) *Tetrahedron Lett.* **39,** 5401–5404
24. Obika, S., Andoh, J., Sugimoto, T., Miyashita, K., and Imanishi, T. (1999) *Tetrahedron Lett.* **40,** 6465–6468
25. Imanishi, T., and Obika, S. (1999) *J. Syn. Org. Chem. Jpn.* **57,** 969–980
26. Obika, S., Hari, Y., Morio, K., and Imanishi, T. (2000) *Tetrahedron Lett.* **41,** 215–219
27. Obika, S., Hari, Y., Morio, K., and Imanishi, T. (2000) *Tetrahedron Lett.* **41,** 221–224
28. Singh, S. K., Nielsen, P., Koshkin, A. A., and Wengel, J. (1998) *Chem. Commun.* 455–456
29. Koshkin, A. A., Singh, S. K., Nielsen, P., Rajwanshi, V. K., Kumar, R., Meldgaard, M., Olsen, C. E., and Wengel, J. (1998) *Tetrahedron* **54,** 3607–3630
30. Obika, S., Morio, K., Nanbu, D., and Imanishi, T. (1997) *Chem. Commun.* 1643–1644
31. Obika, S., Morio, K., Hari, Y., and Imanishi, T. (1999) *Chem. Commun.* 2423–2424
32. Obika, S., Morio, K., Hari, Y., and Imanishi, T. (1999) *Bioorg. Med. Chem. Lett.* **9,** 515–518
33. Lyamichev, V. I., Mirkin, S. M., Frank-Kamenetskii, M. D., and Cantor, C. R. (1988) *Nucleic Acids Res.* **16,** 2165–2178
34. Torigoe, H., Ferdous, A., Watanabe, H., Akaike, T., and Maruyama, A. (1999) *J. Biol. Chem.* **274,** 6161–6167
35. Langerman, N., and Biltonen, R. L. (1979) *Methods Enzymol.* **61,** 261–286
36. Biltonen, R. L., and Langerman, N. (1979) *Methods Enzymol.* **61,** 287–318
37. Wiseman, T., Williston, S., Brandts, J. F., and Lin, L.-N. (1989) *Anal. Biochem.* **179,** 131–137
38. Kamiya, M., Torigoe, H., Shindo, H., and Sarai, A. (1996) *J. Am. Chem. Soc.* **118,** 4532–4538
39. Torigoe, H., Shimizume, R., Sarai, A., and Shindo, H. (1999) *Biochemistry* **38,** 14653–14659
40. Torigoe, H., Ferdous, A., Watanabe, H., Akaike, T., and Maruyama, A. (1999) *Nucleosides, Nucleotides & Nucleic Acids* **18,** 1655–1656
41. Cush, R., Cronin, J. M., Stewart, W. J., Maule, C. H., Molloy, J., and Goddard, N. J. (1993) *Biosens. Bioelectron.* **8,** 347–353
42. Edwards, P. R., Gill, A., Pollard-Knight, D. V., Hoare, M., Buckle, P. E., Lowe, P. A., and Leatherbarrow, R. J. (1995) *Anal. Biochem.* **231,** 210–217
43. Bates, P. J., Dosanjh, H. S., Kumar, S., Jenkins, T. C., Laughton, C. A., and Neidle, S. (1995) *Nucleic Acids Res.* **23,** 3627–3632
44. Manzini, G., Xodo, L. E., Gasparotto, D., Quadrifoglio, F., van der Marel, G. A., and van Boom, J. H. (1990) *J. Mol. Biol.* **213,** 833–843
45. Johnson, K. H., Gray, D. M., and Sutherland, J. C. (1991) *Nucleic Acids Res.* **19,** 2275–2280
46. Edelhoch, H., and Osborne, J. C., Jr. (1976) *Adv. Protein Chem.* **30,** 183–250
47. Cheng, Y.- K., and Pettitt, B. M. (1992) *Prog. Biophys. Mol. Biol.* **58,** 225–257
48. Shafer, R. H. (1998) *Prog. Nucleic Acids Res. Mol. Biol.* **59,** 55–94
49. Rougee, M., Faucon, B., Mergny, J. L., Barcelo, F., Giovannangeli, C., Garestier, T., and Helene, C. (1992) *Biochemistry* **31,** 9269–9278